

CCF: Complementary Collaborative Fusion for Domain Generalized Multi-Modal 3D Object Detection

Yuchen Wu, Kun Wang, Yining Pan, Na Zhao*

Singapore University of Technology and Design

{yuchen_wu, yining_pan}@mymail.sutd.edu.sg, {kun_wang, na_zhao}@sutd.edu.sg

Abstract

Multi-modal fusion has emerged as a promising paradigm for accurate 3D object detection. However, performance degrades substantially when deployed in target domains different from training. In this work, focusing on dual-branch proposal-level detectors, we identify two factors that limit robust cross-domain generalization: 1) in challenging domains such as rain or nighttime, one modality may undergo severe degradation; 2) the LiDAR branch often dominates the detection process, leading to systematic underutilization of visual cues and vulnerability when point clouds are compromised. To address these challenges, we propose three components. First, Query-Decoupled Loss provides independent supervision for 2D-only, 3D-only, and fused queries, rebalancing gradient flow across modalities. Second, LiDAR-Guided Depth Prior augments 2D queries with instance-aware geometric priors through probabilistic fusion of image-predicted and LiDAR-derived depth distributions, improving their spatial initialization. Third, Complementary Cross-Modal Masking applies complementary spatial masks to the image and point cloud, encouraging queries from both modalities to compete within the fused decoder and thereby promoting adaptive fusion. Extensive experiments demonstrate substantial gains over state-of-the-art baselines while preserving source-domain performance. Code and models are publicly available at <https://github.com/IMPL-Lab/CCF.git>.

1. Introduction

3D scene understanding is a core capability for autonomous agents to perceive and interpret complex environments, and has been widely studied in tasks such as 3D object detection [8, 24, 25, 28, 37, 38, 41, 43, 44], 3D semantic segmentation [34, 39, 40, 42], and panoptic scene understanding [13, 19]. Among these tasks, multi-modal 3D object detection [3, 6, 14, 15, 18, 26, 30, 32, 33, 35, 36] constitutes a

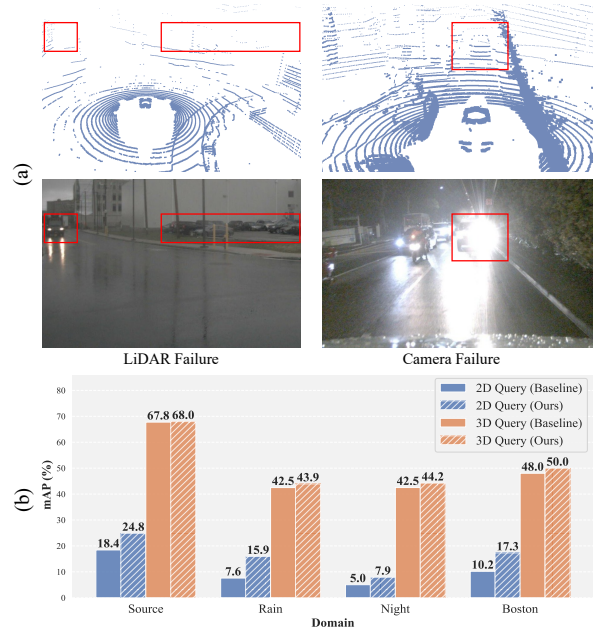


Figure 1. (a) Qualitative examples show that LiDAR and camera modalities degrade differently under adverse conditions. (b) Quantitative results on a baseline dual-branch detector show that our method substantially improves camera-originated queries and narrows their performance gap to LiDAR-originated queries.

pivotal paradigm for scene perception, leveraging the complementary strengths of LiDAR point clouds, which provide accurate geometric structure, and multi-view images, which offer rich semantic context. This heterogeneous modality integration has led to substantially improved detection performance on standard benchmarks. Nevertheless, existing methods largely focus on in-domain optimization and often suffer severe performance degradation when exposed to domain shifts caused by adverse weather, illumination changes, or unseen scene distributions. Given the diverse and dynamic nature of real-world environments, developing robust 3D object detection frameworks with strong cross-domain generalization is crucial for reliable deployment.

*Corresponding Author

In this paper, we identify and address two key factors that contribute to cross-domain fragility. First, adverse weather and lighting conditions degrade sensor observations. As illustrated in Fig. 1 (a), heavy rain causes attenuation and scattering in LiDAR returns, resulting in sparse point clouds for the left and distant vehicles. Meanwhile, low visibility combined with strong glare introduces photometric distortions in camera images, making image-based localization more difficult. Such conditions are rarely represented in training datasets, which are dominated by daytime scenes, leaving models insufficiently prepared for cross-domain deployment. Second, we focus on dual-branch proposal-level detectors, where camera and LiDAR branches generate modality-specific queries before fusion, and observe that existing methods exhibit modality imbalance with reliance on the LiDAR branch. As shown in Fig. 1 (b), detection performance with 2D queries is consistently lower than 3D queries across all evaluated domains, indicating that the semantic information in images is not fully utilized. As a result, when LiDAR quality deteriorates, detection performance can degrade sharply, revealing a critical weakness in the robustness of current multi-modal frameworks.

To address the aforementioned challenges, we propose CCF (Complementary Collaborative Fusion), a systematic framework designed to mitigate modality imbalance and enhance cross-domain robustness. Our approach consists of three components. First, to mitigate supervision imbalance, **Query Decoupled Loss** provides independent learning pathways for 2D-only, 3D-only, and fused queries with three parallel, weight-shared decoder passes. This ensures that image-based queries receive dedicated gradient flow, preventing them from being overshadowed by their 3D counterparts. Second, to improve the geometric accuracy of 2D proposals, **LiDAR-Guided Depth Prior** adaptively fuses learned image-based depth estimates with direct geometric priors from LiDAR points, significantly enhancing 2D query initialization. Finally, to ensure these enhanced and well-supervised queries are effectively utilized during fusion, **Complementary Cross-Modal Masking** introduces a novel augmentation strategy that applies complementary spatial masks to both image and point cloud modalities. This design simulates localized sensor degradations commonly observed under adverse conditions and, more importantly, forces queries from both modalities to compete within the fused decoder, thereby promoting adaptive fusion and preventing over-reliance on any single modality.

Our contributions are summarized as follows:

- We identify and analyze the modality imbalance problem in dual-branch multi-modal 3D detectors, showing that camera-originated queries are systematically under-utilized in supervision, initialization, and fusion.
- We propose CCF (Complementary Collaborative Fusion), a unified framework that improves balanced modality uti-

lization through Query Decoupled Loss, LiDAR-Guided Depth Prior, and Complementary Cross-Modal Masking.

- Extensive experiments on a realistic nuScenes-based domain shift benchmark demonstrate state-of-the-art cross-domain performance and consistent robustness gains across diverse target domains.

2. Related Works

2.1. Multi-Modal Fusion For 3D Object Detection

Multi-modal 3D object detection methods can be broadly grouped by how object representations are formed. One line of work first builds a shared multi-modal representation and then performs decoding with unified object queries. BEVFusion [18] projects both modalities into a common BEV space, while TransFusion [1] and CMT [35] further perform object reasoning with transformer-based queries on fused features. In contrast, proposal-driven methods explicitly maintain modality-specific object hypotheses before fusion. F-PointNet [22] uses 2D detections to guide 3D object search in point clouds, while MV2DFusion [30] generates 2D and 3D proposals from separate branches and refines them jointly with multi-modal features. This explicit dual-branch design provides a natural basis for studying the imbalance between camera- and LiDAR-originated queries.

2.2. Robust Multi-Modal 3D Object Detection

Although multi-modal detectors have achieved strong performance in standard benchmarks, improving their robustness remains crucial for real-world autonomous driving. Existing robust multi-modal 3D detection methods mainly focus on sensor corruption or missing-modality scenarios. MetaBEV [7] introduces a modality-arbitrary BEV decoder that updates meta-BEV queries from available sensors via cross-modal deformable attention. UniBEV [29] introduces channel-normalized weighted fusion for robust feature aggregation when one modality is unavailable. CMT [35] adopts sensor dropout as data augmentation to improve robustness against sensor failures. MEFoformer [4] proposes modality-agnostic decoding to reduce over-reliance on LiDAR, while MoME [21] employs parallel expert decoders to decouple modality dependencies under sensor-failure settings. In contrast, our work addresses domain shifts induced by environmental changes, where both modalities remain available but exhibit different reliability. Such a setting requires not only robustness to degradation, but also balanced utilization of camera and LiDAR information, which is largely overlooked by prior methods.

2.3. Data Augmentation for 3D Perception

Data augmentation creates diverse training distributions that improve robustness to noise and bias in real-world environments. PolarMix [31] enriches point cloud distribu-

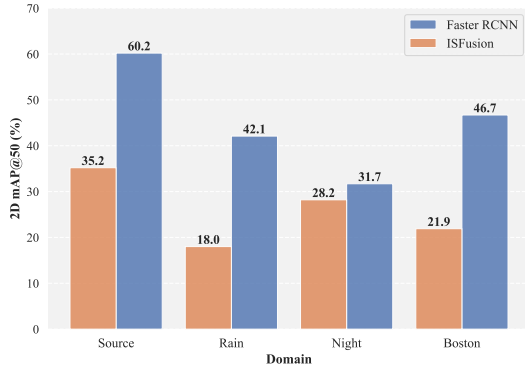


Figure 2. Analysis of 2D proposal quality. We compare the 2D mAP@50 of proposals from the 2D detector (Faster R-CNN) against projected 3D boxes from the 3D detector (ISFusion). The results show that native 2D proposals consistently outperform projected 3D proposals across all domains.

tions through cross-scan mixing, while LaserMix [12] exchanges LiDAR beams across inclination ranges. Park et al. [20] learn erase patterns to mimic point drop under adverse weather. Unlike these methods, our augmentation is not designed to simply simulate corruption patterns, but to reshape the competition between camera- and LiDAR-based queries under complementary partial observations.

3. Pilot Study: Unveiling Modality Imbalance

Dual-branch detectors have demonstrated competitive performance by explicitly leveraging modality-specific proposals [30, 32]. However, their performance under domain shift remains underexplored. To investigate this, we conduct a pilot study on a representative framework: MV2DFusion [30] equipped with ISFusion [36] as the 3D proposal generator and Faster R-CNN [23] as the 2D proposal generator, both trained on our source domain (clear daytime Singapore) and evaluated across all splits. Preliminary observation reveals a striking imbalance: when evaluated separately, 2D-originated queries achieve only 18.44% 3D mAP on the source domain, while 3D-originated queries reach 67.75% mAP. To explain this gap, we first analyze the 2D branch potential, and then examine two limiting factors: supervision imbalance and inaccurate depth estimation.

Untapped 2D Proposal Quality. We first examine whether the quality of initial proposals accounts for the observed performance gap between 2D and 3D queries. To isolate proposal quality from downstream fusion effects, we project 3D boxes predicted by ISFusion onto the image plane and evaluate their 2D Average Precision (AP) against Faster R-CNN. As shown in Fig. 2, image proposals maintain consistently high 2D AP across all domains, surpassing projected 3D boxes from ISFusion. This indicates that 2D proposals retain strong semantic quality even under domain shift.

Imbalanced Training Supervision. To better understand this underutilization, we examine the supervision allocation induced by Hungarian matching during training. Specifically, we count the matched 2D, 3D, and fused queries over 20 training epochs on the source domain. The resulting statistics reveal a pronounced supervision imbalance: each training sample produces, on average, 9.375 matched 3D queries but only 0.25 matched 2D queries, corresponding to a 37.5:1 ratio. This result shows that 3D queries overwhelmingly dominate the assignment process and therefore receive substantially stronger gradient supervision.

Inaccurate Depth Estimation. Beyond semantic quality and supervision imbalance, we further examine whether inaccurate depth estimation limits the effectiveness of 2D queries, since depth initialization is critical for 3D localization. In dual-branch frameworks [30, 32], 2D queries estimate depth from image ROI features using a learned predictor, without explicit geometric constraints. To quantify this limitation, we measure the Mean Absolute Error (MAE) of matched 2D-query depth predictions against ground-truth 3D boxes over the 0–40 m range across all domains. The results reveal substantial errors even on the source domain, with an MAE of 1.78 m, and the error further increases under domain shift to 3.01 m on Rain, 2.27 m on Night, and 2.55 m on Boston. These findings indicate that purely image-based depth prediction introduces considerable localization uncertainty under challenging conditions. This observation also suggests a natural direction for improvement: leveraging LiDAR-derived geometric priors to provide more reliable depth cues for 2D queries.

Key Findings. Our pilot study yields three key observations: (1) image proposals retain strong untapped potential, exhibiting high 2D detection quality across domains; (2) supervision is disproportionately allocated to 3D queries, leaving 2D queries insufficiently optimized; and (3) inaccurate depth estimation further limits the 3D localization capability of 2D queries. Together, these findings motivate the design of mechanisms that *improve 2D query initialization* with geometric cues and *rebalance supervision* during training. We introduce these components in Sec. 4.

4. Method

In this section, we present CCF, a framework designed to mitigate the modality imbalance identified in Sec. 3. We begin by revisiting the baseline dual-branch architecture (Sec. 4.1) to establish necessary notation and context. We then introduce three components: **Query Decoupled Loss** (Sec. 4.2) to provide balanced supervision across modality-specific queries, **LiDAR-Guided Depth Prior** (Sec. 4.3) to enhance 2D query initialization with geometric cues, and **Complementary Cross-Modal Masking** (Sec. 4.4) to encourage complementary learning during fusion.

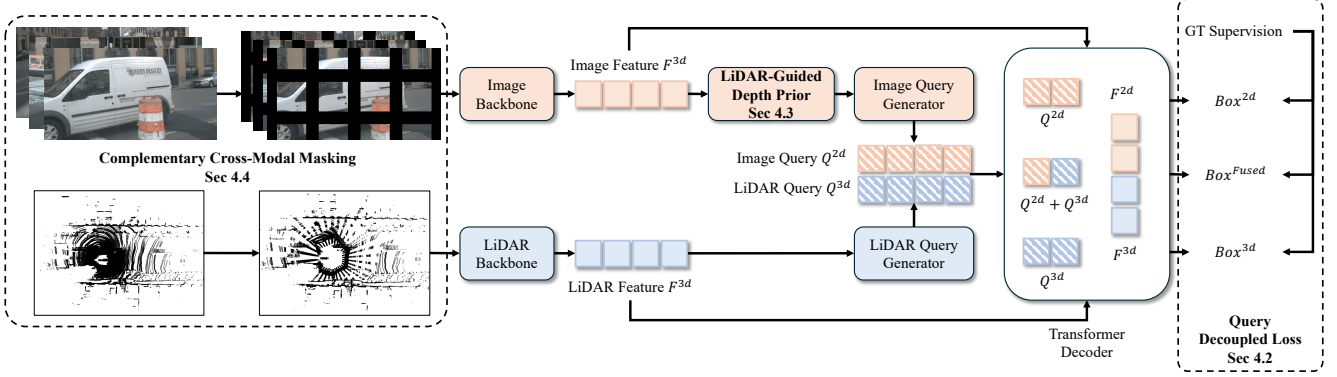


Figure 3. **Overview of CCF.** CCF addresses modality imbalance with three components. (a) **Query Decoupled Loss** uses three parallel, weight-shared decoder passes (2D-only, 3D-only, and fused) to provide modality-specific supervision while avoiding shortcut learning. (b) **LiDAR-Guided Depth Prior** adaptively fuses image-predicted and LiDAR-derived depth distributions to improve 2D query initialization. (c) **Complementary Cross-Modal Masking** applies complementary spatial masking, encouraging balanced competition between camera- and LiDAR-originated queries. Together, these components improve modality balance and robustness under domain shift.

4.1. Revisiting Dual-Branch Detection

Our method builds upon the dual-branch detection framework MV2DFusion [30], which follows a two-stage pipeline: (1) modality-specific proposal generation, and (2) query-based fusion. A 2D detector produces M^{2d} 2D proposals $\mathbf{b}^{2d} \in \mathbb{R}^{M^{2d} \times 4}$, while a 3D detector generates M^{3d} 3D proposals $\mathbf{b}^{3d} \in \mathbb{R}^{M^{3d} \times 7}$. These proposals are then converted into queries for fusion.

Query Formulation. Each 3D proposal generates a query $\mathbf{q}^{3d} = (\mathbf{c}^{3d}, \mathbf{r}^{3d})$, where $\mathbf{c}^{3d} \in \mathbb{R}^{M^{3d} \times C}$ contains RoI appearance and geometric features, and $\mathbf{r}^{3d} \in \mathbb{R}^{M^{3d} \times 3}$ takes the centers of \mathbf{b}^{3d} as reference points. Each 2D proposal produces a query $\mathbf{q}^{2d} = (\mathbf{c}^{2d}, \mathbf{r}^{2d})$, where $\mathbf{c}^{2d} \in \mathbb{R}^{M^{2d} \times C}$ encodes RoI features, and $\mathbf{r}^{2d} \in \mathbb{R}^{M^{2d} \times 3}$ represents estimated 3D positions derived from depth prediction.

Decoder and Training. Combined queries $\mathbf{q}^0 = (\mathbf{q}^{2d}, \mathbf{q}^{3d})$ are processed through a transformer decoder with L layers, producing refined queries \mathbf{q}^L for final 3D box prediction. Training employs Hungarian matching to assign queries to ground truth. As revealed in Sec. 3, this standard training leads to severe imbalance where 3D queries dominate matching, leaving 2D queries insufficiently supervised.

4.2. Query Decoupled Loss

As revealed in Sec. 3, 3D queries dominate Hungarian matching during training and therefore receive substantially more supervision than 2D queries. This imbalance limits the gradient signal reaching the image branch and weakens its optimization. Although both query types are matched under the same assignment rule, the superior localization quality of 3D queries, inherited from LiDAR geometry, allows them to capture most ground-truth assignments. As a result, 2D queries receive insufficient supervision to im-

prove their own localization quality, further reinforcing the imbalance. To mitigate this issue, we propose Query Decoupled Loss, which provides independent supervision for each modality and thereby rebalances the training process.

Decoupled Decoder Architecture. A straightforward alternative is to decode the fused queries \mathbf{q}^L in a single pass and then separate them by modality for independent loss computation. However, this design introduces a shortcut: during self-attention, 2D queries can rely on information propagated from co-attending 3D queries, rather than being optimized as an independent query set. To avoid this issue, we execute the decoder *three times in parallel* with shared weights: (1) a *2D-only pass* operating on $\mathbf{q}^{2d,0}$, (2) a *3D-only pass* operating on $\mathbf{q}^{3d,0}$, and (3) a *fused pass* operating on the concatenated query set $\mathbf{q}^0 = (\mathbf{q}^{2d,0}, \mathbf{q}^{3d,0})$. All three passes attend to the same multi-modal feature tokens, while maintaining separate query sets in self-attention. During inference, only the fused pass is used for prediction, introducing no additional computational cost.

Loss Formulation. Each decoder pass produces refined queries: $\mathbf{q}^{2d,L}$ from the 2D-only pass, $\mathbf{q}^{3d,L}$ from the 3D-only pass, and \mathbf{q}^L from the fused pass. Independent Hungarian matching and losses are applied to each output:

$$\mathcal{L}_{\text{total}} = \mathcal{L}_{2d} + \mathcal{L}_{3d} + \mathcal{L}_{\text{fused}}, \quad (1)$$

where each component consists of classification and box regression terms:

$$\mathcal{L}_{(\cdot)} = \mathcal{L}_{\text{cls}}^{(\cdot)} + \mathcal{L}_{\text{box}}^{(\cdot)}. \quad (2)$$

We adopt focal loss [16] for \mathcal{L}_{cls} and L1 loss for \mathcal{L}_{box} , following the baseline. Importantly, the 2D-only branch ensures that 2D queries receive direct supervision by competing only within the 2D query set, while the fused branch preserves the full capability of the original framework.

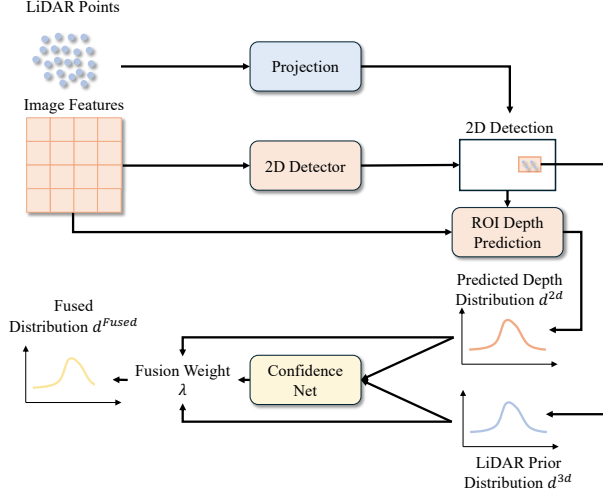


Figure 4. **Illustration of our LiDAR-Guided Depth Prior.** For each 2D proposal, we extract a learned depth distribution from image features (\mathbf{d}^{2d}) and a geometric prior from LiDAR points (\mathbf{d}^{3d}). A confidence network adaptively predicts a fusion weight (λ) to combine them into a fused distribution (\mathbf{d}^{Fused}), which provides robust depth initialization for the 2D query.

4.3. LiDAR-Guided Depth Prior

While Query Decoupled Loss improves the supervision received by 2D queries in isolation, it does not address the fundamental quality issue identified in Sec. 3: inaccurate depth estimation still severely limits their 3D localization capability. Consequently, even under balanced supervision, poorly initialized 2D queries remain less competitive than 3D queries in the fused branch. In multi-modal detection, however, LiDAR points within 2D proposals can provide informative estimates of the underlying object depth distribution. Motivated by this observation, we leverage LiDAR-derived geometric priors to enhance 2D query initialization and improve their effectiveness during fusion.

Dual-Source Depth Distributions. As illustrated in Fig. 4, for each 2D proposal \mathbf{b}_i^{2d} , we estimate depth from two complementary sources. From the image branch, a lightweight depth predictor processes RoI features and outputs a probability distribution $\mathbf{d}_i^{2d} \in \mathbb{R}^D$ over D depth bins. From the LiDAR branch, we collect points inside the 3D frustum defined by \mathbf{b}_i^{2d} and discretize their depths into a histogram. If no LiDAR points fall inside the frustum, we use a uniform distribution by default. The normalized histogram forms a geometric prior distribution $\mathbf{d}_i^{3d} \in \mathbb{R}^D$. This LiDAR-derived prior provides explicit geometric evidence, although it may become sparse or noisy for distant objects or under adverse conditions such as rain.

Adaptive Distribution Fusion. Simply averaging or concatenating these two distributions is suboptimal, since their

reliability varies across instances. For example, image-based depth may be more reliable for distant objects with sparse LiDAR support, whereas the LiDAR prior is often more accurate for nearby objects with sufficient point coverage. To address this issue, we introduce a confidence network that adaptively fuses these complementary distributions. Given \mathbf{d}_i^{2d} and \mathbf{d}_i^{3d} , this lightweight network predicts an instance-specific fusion weight $\lambda_i \in [0, 1]$. The fused depth distribution is then computed as

$$\mathbf{d}_i^{fused} = \sigma(\lambda_i \cdot \log(\mathbf{d}_i^{2d}) + (1 - \lambda_i) \cdot \log(\mathbf{d}_i^{3d})), \quad (3)$$

where $\sigma(\cdot)$ denotes the softmax function. This log-space fusion, analogous to a Product-of-Experts [9], allows the model to emphasize the more reliable depth source for each instance. We then compute the expected depth from \mathbf{d}_i^{fused} and use it to initialize the 3D reference point \mathbf{r}_i^{2d} of the corresponding 2D query, thereby improving its localization.

4.4. Complementary Cross-Modal Masking

While the previous two components strengthen 2D queries through dedicated supervision and improved initialization, a critical challenge remains in the fused branch: 3D queries still dominate Hungarian matching in the fused branch. The decoder learns to rely heavily on consistently accurate 3D queries, limiting its ability to adaptively leverage 2D queries when conditions favor them. To address this, we need an augmentation strategy that forces the decoder to utilize queries from both modalities during training, preparing it to make adaptive selections at test time based on domain-specific modality reliability.

Complementary Cross-Modal Masking. In real-world domain shifts, modalities often degrade differently: rain obscures LiDAR while cameras remain informative, whereas low-light conditions degrade images while LiDAR maintains geometric coverage. This complementary degradation pattern suggests that two modalities should be augmented complementarily rather than uniformly during training. We simulate this through complementary spatial masking at the input level. Given a spatial mask $\mathbf{M} \in \{0, 1\}^{H \times W}$ on the image plane, we mask the raw image \mathbf{I} by setting pixels with $\mathbf{M} = 0$ to zero. For the LiDAR point cloud $\mathbf{P} = \{\mathbf{p}_i\}_{i=1}^N$, we project each point onto the image plane via camera intrinsics \mathbf{K} and extrinsics $[\mathbf{R}|\mathbf{t}]$:

$$[u_i, v_i, 1]^\top \propto \mathbf{K}(\mathbf{R}\mathbf{p}_i + \mathbf{t}), \quad (4)$$

and retain only the points whose projected locations fall in the complementary masked regions. In this way, when one modality is masked at a spatial location, the other modality is explicitly retained. Unlike consistent masking that degrades both modalities simultaneously, our design encourages more balanced competition between camera- and LiDAR-originated queries under partial observations.

For mask generation, we adopt GridMask [5], following the 2D augmentation protocol used in CMT [35], to produce structured spatial masks. To stabilize training, we use a curriculum schedule in which the masking probability increases linearly from 0 to p during training. This allows the model to first learn from complete multi-modal observations before progressively adapting to partial inputs. The masked images and filtered point clouds are then fed into their respective feature extractors prior to query generation.

Benefits for Adaptive Query Selection. This strategy better reflects real-world domain shifts in which the two modalities degrade asymmetrically, such as LiDAR sparsity in rain and visual degradation at night. By training with complementary partial observations, the decoder learns to adaptively select and balance camera- and LiDAR-originated queries according to their reliability. Unlike complete modality dropout in CMT, our approach preserves both modalities with complementary visibility patterns, better matching practical test conditions where both sensors remain available but differ in quality.

5. Experiments

5.1. Experimental Setup

Dataset and Domain Splits. We build our benchmark on nuScenes [2] by defining domain splits according to natural environmental attributes. The **source domain** consists of 226 clear daytime Singapore scenes. We consider three **target domains** from the validation set: *Rain* (27 scenes), *Night* (15 scenes), and *Boston* (77 scenes), covering naturally occurring weather, illumination, and geographic shift.

Implementation Details. We implement CCF on top of the MV2DFusion architecture [30], using ISFusion [36] and Faster R-CNN [23] as the LiDAR and image query generators, respectively, followed by a 6-layer fusion decoder. Query Decoupled Loss uses identical weights across the 2D-only, 3D-only, and fused branches. LiDAR-Guided Depth Prior employs $D = 25$ bins with a 3-layer MLP confidence network. Complementary Cross-Modal Masking adopts GridMask [5] with curriculum learning, increasing masking probability from 0 to $p = 0.7$.

Training Procedure. To prevent data leakage and ensure fair evaluation, we adopt a two-stage training strategy. In *Stage 1*, both proposal generators are pre-trained exclusively on the source domain. Specifically, the 2D detector (Faster R-CNN) is trained using 2D bounding boxes obtained by projecting source-domain 3D annotations onto image planes, rather than nuImages pre-trained weights that may contain target-domain scenes. The 3D detector (ISFusion) is trained on the source split of nuScenes. In *Stage 2*, we freeze the 3D proposal generator and train the fusion decoder for 24 epochs with a batch size of 16 us-

ing the AdamW optimizer [11], an initial learning rate of 4×10^{-4} , weight decay of 0.01, and a cosine annealing schedule. Standard data augmentations, including random flipping, rotation, and scaling, are applied during training.

Evaluation Metrics. We report two metrics: (1) **mAP** (mean Average Precision), averaged over 10 object classes, and (2) **NDS** (nuScenes Detection Score) [2], which combines mAP with translation, scale, orientation, velocity, and attribute errors. Higher values indicate better performance. Owing to the natural data distribution, some target domains do not contain all object categories (*e.g.*, the Night split contains no trailer, construction vehicle, or bus instances). Nevertheless, we report metrics over all 10 classes to remain consistent with the standard nuScenes evaluation protocol.

Baselines and Comparisons. We compare against representative multi-modal 3D detectors that fuse LiDAR and camera information, including CMT [35], MOAD [4], MEFormer [4], ISFusion [36], and MoME [21]. For reference, we also include FSDv2 [15], a LiDAR-only detector representing single-modality performance. Our method follows a proposal-level fusion paradigm in which modality-specific proposals are generated before cross-modal fusion, with MV2DFusion [30] serving as the base framework. For fair comparison, all methods are evaluated under the same data splits, training procedures, and evaluation protocols.

5.2. Main Results

Tab. 1 summarizes the cross-domain detection performance of our method and prior baselines. On the source domain, our method remains competitive, achieving 68.2% mAP, which indicates that the proposed training strategy preserves in-domain performance. Under domain shift, however, it consistently yields clear gains, improving mAP by **+2.8%** on Rain, **+1.3%** on Night, and **+3.2%** on Boston. These results support our claim that improving modality balance is important for robust cross-domain generalization.

Comparison with Multi-Modal Baselines. Existing multi-modal detectors show reasonable source-domain accuracy but degrade substantially on unseen domains. This trend is particularly evident for methods based on unified feature or query representations, suggesting that they are less effective at preserving modality-specific cues when sensor reliability changes across domains. In contrast, our method is designed to retain modality-specific proposals and strengthen their interaction during fusion, leading to better target-domain robustness.

Our Approach and Improvements. Compared with the baseline, our method improves target-domain mAP by 2.8/1.3/3.2 points on Rain/Night/Boston, while maintaining comparable performance on the source domain. These gains come from three complementary components: Query Decoupled Loss strengthens modality-specific su-

Table 1. Main results on nuScenes domain generalization splits. We report mAP (%) and NDS (%) on the source domain (Src) and three target domains (Rain, Night, Boston). Average is computed over Rain/Night/Boston. L and C denote LiDAR and Camera, respectively. † represents the model trained with nuScenes full split.

Model	Reference	Modality	Source		Rain		Night		Boston		Average	
			mAP	NDS								
FSDv2 [15]	TPAMI 24	L	59.6	62.7	23.4	41.6	36.6	42.8	28.2	45.1	29.4	43.2
CMT [35]	ICCV 23	L+C	61.4	62.3	35.7	46.5	37.8	42.0	42.1	50.8	38.5	46.4
MOAD [4]	arXiv 24	L+C	64.1	64.4	39.2	49.4	41.1	44.3	43.9	53.0	41.4	48.9
MEFormer [4]	arXiv 24	L+C	63.4	63.7	40.1	50.1	41.1	44.0	44.3	53.0	41.8	49.0
ISFusion [36]	CVPR 24	L+C	66.3	65.4	39.8	49.4	41.8	45.1	45.4	53.4	42.3	49.3
MoME [21]	CVPR 25	L+C	63.6	64.0	37.7	48.5	39.5	43.3	42.9	52.4	40.0	48.1
Our baseline	-	L+C	68.4	65.7	41.9	50.0	42.9	44.5	47.4	53.6	44.1	49.4
CCF (Ours)	-	L+C	68.2	65.9	44.7	52.5	44.2	45.3	50.6	56.8	46.5	51.5
CCF (Oracle) [†]	-	L+C	73.6	74.2	72.9	74.5	46.9	48.3	73.6	74.8	64.5	65.9

Table 2. Oracle results on nuScenes domain generalization splits.

Models	All		Rain		Night	
	mAP	NDS	mAP	NDS	mAP	NDS
BEVDet [10]	34.9	41.7	30.1	43.2	12.0	21.7
PETR [17]	37.0	44.2	41.9	50.6	17.2	24.2
CenterPoint [37]	59.6	66.8	59.2	-	35.4	-
FSDv2 [15]	64.7	70.4	61.1	68.8	37.1	43.6
Transfusion-L [1]	65.1	70.1	64.0	69.9	37.5	43.5
Transfusion [1]	67.3	71.2	67.5	71.9	39.8	44.7
BEVFusion [18]	68.5	71.4	69.9	-	42.8	-
GraphBEV [27]	70.1	72.9	70.2	-	45.1	-
CMT [35]	70.3	72.9	70.5	73.7	42.8	46.3
MOAD [4]	71.3	73.7	72.3	74.6	42.8	46.5
MEFormer [4]	71.5	73.9	72.3	75.0	43.5	46.9
ISFusion [36]	72.7	73.8	72.8	74.8	45.0	47.4
MoME [21]	71.2	73.6	72.1	74.6	42.7	46.5
MV2DFusion [30]	70.2	72.7	69.8	73.4	44.9	47.2
Ours	73.6	74.2	72.9	74.5	46.9	48.3

pervision, LiDAR-Guided Depth Prior improves the spatial initialization of image queries, and Complementary Cross-Modal Masking promotes more balanced competition between camera- and LiDAR-originated queries. This trend is also reflected in Fig. 1(b), where camera-originated queries show substantially larger gains, narrowing the gap to LiDAR-originated queries under domain shift. Beyond mAP, our method also achieves consistently stronger NDS across all domains, indicating improved overall detection quality. Qualitative examples in Fig. 5 further show fewer missed detections and false positives.

To understand the upper bound of performance when trained on target domains, we conduct oracle experiments where models are trained on the standard training split. As shown in Tab. 2, our method achieves 73.6/72.9/46.9% mAP on All/Rain/Night splits, outperforming all baselines.

5.3. Ablation Studies

We conduct ablation studies to evaluate the contribution of each component. As shown in Tab. 3, Query Decoupled

Table 3. Ablation studies of the proposed components. We evaluate Query Decoupled Loss (DL), LiDAR-Guided Depth Prior (DP), and Complementary Cross-Modal Masking (CM), and report mAP (%) and NDS (%) on all domains.

Components			Source		Rain		Night		Boston	
DL	DP	CM	mAP	NDS	mAP	NDS	mAP	NDS	mAP	NDS
X	X	X	68.4	65.7	41.9	50.0	42.9	44.5	47.4	53.6
X	✓	X	68.6	66.0	42.3	50.6	41.8	44.4	47.5	53.8
X	X	✓	68.4	65.8	44.5	51.4	43.4	45.2	49.6	56.4
X	✓	✓	68.7	66.1	44.7	51.5	44.1	45.4	49.7	56.3
✓	X	X	68.4	66.1	42.8	52.4	42.1	44.7	48.1	56.0
✓	✓	X	68.8	66.4	44.7	53.6	42.2	44.6	50.0	56.9
✓	X	✓	68.4	66.2	44.3	51.2	43.9	45.8	50.2	56.9
✓	✓	✓	68.2	65.9	44.7	52.5	44.2	45.3	50.6	56.8

Loss improves performance on Rain and Boston, suggesting that stronger modality-specific supervision benefits cross-domain generalization when image cues remain informative. However, it causes a slight drop on Night, where LiDAR is generally more reliable than degraded camera observations. LiDAR-Guided Depth Prior shows a similar trend, as both components primarily strengthen the image branch. In contrast, Complementary Cross-Modal Masking brings consistent gains even without Query Decoupled Loss, indicating that exposing the model to complementary modality degradation is itself effective for improving robustness. When combined with the other components, it further encourages adaptive query selection based on modality reliability rather than fixed preference. Overall, the full model achieves the strongest target-domain mAP performance across the three target splits.

Masking Strategy Design. We further analyze the design choices of cross-modal masking in Tab. 4. Starting from the baseline with standard image GridMask [5], we compare several masking variants. *Modal Mask*, following CMT [35] by completely dropping one modality, yields only limited gains because it does not expose the model



Figure 5. Examples of 3D object detections on different data splits. We visualize the 3D bounding boxes of car, truck and pedestrian with orange, magenta and blue colors in the multi-view images.

Table 4. Ablation studies on Complementary Cross-Modal Mask variants. ‘‘Cur.’’ indicates whether curriculum learning is applied.

Configuration			Rain		Night		Boston	
Variant	Cur.	mAP	NDS	mAP	NDS	mAP	NDS	
(a) Image GridMask	✗	42.8	50.7	42.5	45.3	48.3	54.7	
(b) Modal Mask	✗	42.9	49.7	42.6	44.5	48.4	55.4	
(c) Consistent GridMask	✗	42.8	49.8	42.2	44.3	48.9	55.5	
(d) Complementary GridMask	✗	43.9	50.0	43.1	44.2	49.2	55.1	
(e) Complementary RandomMask	✓	44.1	51.1	44.1	46.0	49.7	55.2	
(f) Complementary GridMask	✓	44.3	51.2	43.9	45.8	50.2	56.9	

to complementary partial observations from both modalities. *Consistent GridMask*, which applies the same mask to image and LiDAR inputs, also brings only marginal improvement, as it degrades both modalities simultaneously and thus provides limited support for adaptive fusion. In contrast, *Complementary GridMask* consistently performs better, confirming the importance of preserving complementary observations across modalities. Adding curriculum learning further improves performance, suggesting that progressively increasing masking difficulty stabilizes optimization by allowing the model to first learn from complete inputs and then adapt to partial observations. Replacing GridMask with random masking produces similar results, indicating that the key benefit comes from cross-modal complementarity rather than the specific mask pattern.

6. Conclusions

In this work, we study domain generalization for multi-modal 3D object detection in dual-branch proposal-level detectors. We identify modality imbalance as a key limitation of this paradigm: camera-originated queries are often underutilized due to weaker supervision and less reliable spatial initialization, which becomes particularly detrimental under domain shift. To address this issue, we propose Complementary Collaborative Fusion (CCF), a unified framework consisting of Query Decoupled Loss, LiDAR-Guided Depth Prior, and Complementary Cross-Modal Masking. Extensive experiments on challenging real-world domain shifts demonstrate that CCF consistently improves cross-domain robustness over strong baselines while preserving competitive source-domain performance. These results further show the importance of balanced supervision and adaptive query selection for robust multi-modal perception.

Acknowledgments

This work was supported in part by the Ministry of Education, Singapore, under its MOE Academic Research Fund Tier 2 (MOE-T2EP20124-0013), and the Agency for Science, Technology and Research (A*STAR) under its MTC Programmatic Funds (Grant No. M23L7b0021). This research work is also supported by Temasek Labs@SUTD.

References

- [1] Xuyang Bai, Zeyu Hu, Xinge Zhu, Qingqiu Huang, Yilun Chen, Hongbo Fu, and Chiew-Lan Tai. TransFusion: Robust LiDAR-camera fusion for 3D object detection with transformers. In *IEEE/CVF Conference on Computer Vision and Pattern Recognition, CVPR 2022, New Orleans, LA, USA, June 18-24, 2022*, pages 1080–1089. IEEE, 2022. 2, 7
- [2] Holger Caesar, Varun Bankiti, Alex H. Lang, Sourabh Vora, Venice Erin Liong, Qiang Xu, Anush Krishnan, Yuxin Pan, Giancarlo Baldan, and Oscar Beijbom. nuScenes: A multimodal dataset for autonomous driving. *2020 IEEE/CVF Conference on Computer Vision and Pattern Recognition (CVPR)*, pages 11618–11628, 2019. 6
- [3] Qi Cai, Yingwei Pan, Ting Yao, Chong-Wah Ngo, and Tao Mei. Objectfusion: Multi-modal 3d object detection with object-centric fusion. In *2023 IEEE/CVF International Conference on Computer Vision (ICCV)*, pages 18021–18030, 2023. 1
- [4] Juhan Cha, Minseok Joo, Jihwan Park, Sanghyeok Lee, Injae Kim, and Hyunwoo J. Kim. Robust multimodal 3d object detection via modality-agnostic decoding and proximity-based modality ensemble. *arXiv preprint arXiv:2407.19156*, 2024. 2, 6, 7
- [5] Pengguang Chen, Shu Liu, Hengshuang Zhao, and Ji-aya Jia. Gridmask data augmentation. *arXiv preprint arXiv:2001.04086*, 2020. 6, 7
- [6] Xiaozhi Chen, Huimin Ma, Ji Wan, Bo Li, and Tian Xia. Multi-view 3d object detection network for autonomous driving. In *2017 IEEE Conference on Computer Vision and Pattern Recognition (CVPR)*, pages 6526–6534, 2017. 1
- [7] Chongjian Ge, Junsong Chen, Enze Xie, Zhongdao Wang, Lanqing Hong, Huchuan Lu, Zhenguo Li, and Ping Luo. Metabev: Solving sensor failures for 3d detection and map segmentation. In *ICCV*, 2023. 2
- [8] Yucheng Han, Na Zhao, Weiling Chen, Keng Teck Ma, and Hanwang Zhang. Dual-perspective knowledge enrichment for semi-supervised 3d object detection. In *Proceedings of the AAAI Conference on Artificial Intelligence*, pages 2049–2057, 2024. 1
- [9] G.E. Hinton. *Products of experts*, pages 1–6. IEEE, 1999. 5
- [10] Junjie Huang, Guan Huang, Zheng Zhu, Yun Ye, and Dalong Du. BEVDet: High-performance Multi-camera 3D Object Detection in Bird-Eye-View. *arXiv preprint arXiv:2112.11790*, 2022. 7
- [11] Diederik P. Kingma and Jimmy Ba. Adam: A method for stochastic optimization. In *3rd International Conference on Learning Representations, ICLR 2015, San Diego, CA, USA, May 7-9, 2015, Conference Track Proceedings*, 2015. 6
- [12] Lingdong Kong, Jiawei Ren, Liang Pan, and Ziwei Liu. Lasermix for semi-supervised lidar semantic segmentation. In *IEEE/CVF Conference on Computer Vision and Pattern Recognition*, pages 21705–21715, 2023. 3
- [13] Jinke Li, Xiao He, Yang Wen, Yuan Gao, Xiaoqiang Cheng, and Dan Zhang. Panoptic-phnet: Towards real-time and high-precision lidar panoptic segmentation via clustering pseudo heatmap. In *2022 IEEE/CVF Conference on Computer Vision and Pattern Recognition (CVPR)*, pages 11799–11808, 2022. 1
- [14] Wenxuan Li, Qin Zou, Chi Chen, Bo Du, Long Chen, Jian Zhou, and Hongkai Yu. Co-fix3d: Enhancing 3d object detection with collaborative refinement. *IEEE Robotics and Automation Letters*, 10(5):4970–4977, 2025. 1
- [15] Yingyan Li, Lue Fan, Yang Liu, Zehao Huang, Yuntao Chen, Naiyan Wang, and Zhaoxiang Zhang. Fully Sparse Fusion for 3D Object Detection. *IEEE Transactions on Pattern Analysis and Machine Intelligence*, pages 1–15, 2024. 1, 6, 7
- [16] Tsung-Yi Lin, Priya Goyal, Ross B. Girshick, Kaiming He, and Piotr Dollár. Focal loss for dense object detection. *2017 IEEE International Conference on Computer Vision (ICCV)*, pages 2999–3007, 2017. 4
- [17] Yingfei Liu, Tiancai Wang, Xiangyu Zhang, and Jian Sun. PETR: Position embedding transformation for multi-view 3D object detection. In *Computer Vision - ECCV 2022 - 17th European Conference, Tel Aviv, Israel, October 23-27, 2022, Proceedings, Part XXVII*, pages 531–548. Springer, 2022. 7
- [18] Zhijian Liu, Haotian Tang, Alexander Amini, Xingyu Yang, Huizi Mao, Daniela Rus, and Song Han. BEVFusion: Multi-task multi-sensor fusion with unified bird’s-eye view representation. In *IEEE International Conference on Robotics and Automation (ICRA)*, 2023. 1, 2, 7
- [19] Yining Pan, Qiongjie Cui, Xulei Yang, and Na Zhao. How do images align and complement lidar? towards a harmonized multi-modal 3d panoptic segmentation. In *Forty-second International Conference on Machine Learning, ICML 2025, Vancouver, BC, Canada, July 13-19, 2025*. PMLR / OpenReview.net, 2025. 1
- [20] Junsung Park, Kyungmin Kim, and Hyunjung Shim. Rethinking data augmentation for robust lidar semantic segmentation in adverse weather. *arXiv preprint arXiv:2407.02286*, 2024. 3
- [21] Konyul Park, Yecheol Kim, Daehun Kim, and Jun Won Choi. Resilient sensor fusion under adverse sensor failures via multi-modal expert fusion. In *CVPR*, 2025. 2, 6, 7
- [22] C. Qi, W. Liu, Chenxia Wu, Hao Su, and Leonidas J. Guibas. Frustum pointnets for 3d object detection from rgb-d data. *2018 IEEE/CVF Conference on Computer Vision and Pattern Recognition*, pages 918–927, 2017. 2
- [23] Shaoqing Ren, Kaiming He, Ross B. Girshick, and Jian Sun. Faster r-cnn: Towards real-time object detection with region proposal networks. *IEEE Transactions on Pattern Analysis and Machine Intelligence*, 39:1137–1149, 2015. 3, 6
- [24] Hualian Sheng, Sijia Cai, Na Zhao, Bing Deng, Jianqiang Huang, Xian-Sheng Hua, Min-Jian Zhao, and Gim Hee Lee. Rethinking iou-based optimization for single-stage 3d object detection. In *European Conference on Computer Vision*, pages 544–561. Springer, 2022. 1
- [25] Hualian Sheng, Sijia Cai, Na Zhao, Bing Deng, Qiao Liang, Min-Jian Zhao, and Jieping Ye. Ct3d++: Improving 3d object detection with keypoint-induced channel-wise transformer. *International Journal of Computer Vision*, 133(7): 4817–4836, 2025. 1

- [26] Yang Song and Lin Wang. Bico-fusion: Bidirectional complementary lidar-camera fusion for semantic- and spatial-aware 3d object detection. *IEEE Robotics and Automation Letters*, 10(2):1457–1464, 2025. [1](#)
- [27] Ziyang Song, Lei Yang, Shaoqing Xu, Lin Liu, Dongyang Xu, Caiyan Jia, Feiyang Jia, and Li Wang. GraphBEV: Towards robust BEV feature alignment for multi-modal 3D object detection. In *Computer Vision - ECCV 2024 - 18th European Conference, Milan, Italy, September 29-October 4, 2024, Proceedings, Part XXVI*, pages 347–366. Springer, 2024. [7](#)
- [28] Jiangyi Wang and Na Zhao. Uncertainty meets diversity: A comprehensive active learning framework for indoor 3d object detection. In *Proceedings of the Computer Vision and Pattern Recognition Conference*, pages 20329–20339, 2025. [1](#)
- [29] Shiming Wang, Holger Caesar, Liangliang Nan, and Julian FP Kooij. Unibev: Multi-modal 3d object detection with uniform bev encoders for robustness against missing sensor modalities. In *2024 IEEE Intelligent Vehicles Symposium (IV)*, 2024. [2](#)
- [30] Zitian Wang, Zehao Huang, Yulu Gao, Naiyan Wang, and Si Liu. Mv2dfusion: Leveraging modality-specific object semantics for multi-modal 3d detection. *IEEE Transactions on Pattern Analysis and Machine Intelligence*, pages 1–15, 2025. [1](#), [2](#), [3](#), [4](#), [6](#), [7](#)
- [31] Aoran Xiao, Jiaying Huang, Dayan Guan, Kaiwen Cui, Shijian Lu, and Ling Shao. Polarmix: a general data augmentation technique for lidar point clouds. In *Proceedings of the 36th International Conference on Neural Information Processing Systems*, Red Hook, NY, USA, 2022. Curran Associates Inc. [2](#)
- [32] Yichen Xie, Chenfeng Xu, Marie-Julie Rakotosaona, Patrick Rim, Federico Tombari, Kurt Keutzer, Masayoshi Tomizuka, and Wei Zhan. Sparsefusion: Fusing multi-modal sparse representations for multi-sensor 3d object detection. In *2023 IEEE/CVF International Conference on Computer Vision (ICCV)*, pages 17545–17556, 2023. [1](#), [3](#)
- [33] Shaoqing Xu, Dingfu Zhou, Jin Fang, Junbo Yin, Zhou Bin, and Liangjun Zhang. Fusionpainting: Multimodal fusion with adaptive attention for 3d object detection. In *2021 IEEE International Intelligent Transportation Systems Conference (ITSC)*, pages 3047–3054, 2021. [1](#)
- [34] Yating Xu, Conghui Hu, Na Zhao, and Gim Hee Lee. Generalized few-shot point cloud segmentation via geometric words. In *Proceedings of the IEEE/CVF International Conference on Computer Vision*, pages 21506–21515, 2023. [1](#)
- [35] Junjie Yan, Yingfei Liu, Jianjian Sun, Fan Jia, Shuailin Li, Tiancai Wang, and Xiangyu Zhang. Cross Modal Transformer: Towards Fast and Robust 3D Object Detection. In *ICCV*, pages 18222–18232. IEEE, 2023. [1](#), [2](#), [6](#), [7](#)
- [36] Junbo Yin, Jianbing Shen, Runnan Chen, Wei Li, Ruigang Yang, Pascal Frossard, and Wenguan Wang. Is-fusion: Instance-scene collaborative fusion for multimodal 3d object detection. In *CVPR*, 2024. [1](#), [3](#), [6](#), [7](#)
- [37] Tianwei Yin, Xingyi Zhou, and Philipp Krähenbühl. Center-based 3D object detection and tracking. In *IEEE Conference on Computer Vision and Pattern Recognition, CVPR 2021, Virtual, June 19-25, 2021*, pages 11784–11793. Computer Vision Foundation / IEEE, 2021. [1](#), [7](#)
- [38] Na Zhao, Tat-Seng Chua, and Gim Hee Lee. Sess: Self-ensembling semi-supervised 3d object detection. In *Proceedings of the IEEE/CVF Conference on Computer Vision and Pattern Recognition*, pages 11079–11087, 2020. [1](#)
- [39] Na Zhao, Tat-Seng Chua, and Gim Hee Lee. Few-shot 3d point cloud semantic segmentation. In *Proceedings of the IEEE/CVF conference on computer vision and pattern recognition*, pages 8873–8882, 2021. [1](#)
- [40] Na Zhao, Tat-Seng Chua, and Gim Hee Lee. Ps²-net: A locally and globally aware network for point-based semantic segmentation. In *2020 25th International Conference on Pattern Recognition (ICPR)*, pages 723–730. IEEE, 2021. [1](#)
- [41] Na Zhao, Peisheng Qian, Fang Wu, Xun Xu, Xulei Yang, and Gim Hee Lee. Sdcot++: Improved static-dynamic co-teaching for class-incremental 3d object detection. *IEEE Transactions on Image Processing*, 34:4188–4202, 2024. [1](#)
- [42] Yuyang Zhao, Na Zhao, and Gim Hee Lee. Synthetic-to-real domain generalized semantic segmentation for 3d indoor point clouds. In *The British Machine Vision Conference*, 2024. [1](#)
- [43] Yun Zhu, Le Hui, Yaqi Shen, and Jin Xie. Spgroup3d: Superpoint grouping network for indoor 3d object detection. In *Proceedings of the AAAI Conference on Artificial Intelligence*, pages 7811–7819, 2024. [1](#)
- [44] Yun Zhu, Le Hui, Hang Yang, Jianjun Qian, Jin Xie, and Jian Yang. Learning class prototypes for unified sparse-supervised 3d object detection. In *Proceedings of the IEEE/CVF Conference on Computer Vision and Pattern Recognition (CVPR)*, pages 9911–9920, 2025. [1](#)